

High-dimensional atomic microscopy in surface plasmon polaritons

Akhtar Munir, Abdul Wahab, and Munsif Jan

Citation: Chin. Phys. B, 2020, 29 (**12**): 124204. DOI: 10.1088/1674-1056/abbbeb
Journal homepage: http://cpb.iphy.ac.cn; http://iopscience.iop.org/cpb

What follows is a list of articles you may be interested in

High-precision three-dimensional atom localization via probe absorption at room temperature

Mengmeng Luo(罗萌萌), Wenxiao Liu(刘文晓), Dingyu Cai(蔡定宇), and Shaoyan Gao(高韶燕)
Chin. Phys. B, 2020, 29 (**12**): 124205. DOI: 10.1088/1674-1056/abb3df

Electromagnetically induced grating in a thermal N-type four-level atomic system

Ya-Bin Dong(董雅宾), Jun-Yan Li(李俊燕), Zhi-Ying Zhou(周志英)
Chin. Phys. B, 2017, 26 (**1**): 014202. DOI: 10.1088/1674-1056/26/1/014202

Two-dimensional atom localization induced by a squeezed vacuum

Fei Wang(王飞), Jun Xu(徐俊)
Chin. Phys. B, 2016, 25 (**10**): 104201. DOI: 10.1088/1674-1056/25/10/104201

Two-dimensional atom localization via probe absorption in a four-level atomic system

Wang Zhi-Ping, Ge Qiang, Ruan Yu-Hua, Yu Ben-Li
Chin. Phys. B, 2013, 22 (**7**): 074203. DOI: 10.1088/1674-1056/22/7/074203

High-precision two-dimensional atom localization via probe absorption in M-scheme atomic system

Wu Jian-Chun, Liu Zheng-Dong, Zheng Jun
Chin. Phys. B, 2013, 22 (**4**): 044203. DOI: 10.1088/1674-1056/22/4/044203

High-dimensional atomic microscopy in surface plasmon polaritons*

Akhtar Munir[1,2,†], Abdul Wahab[1,2], and Munsif Jan[3,4,‡]

[1] Synergetic Innovation Center of Quantum Information and Quantum Physics, University of Science and Technology of China, Hefei 230026, China
[2] Shanghai Branch, National Laboratory for Physical Sciences at Microscale, University of Science and Technology of China, Shanghai 201315, China
[3] Key Laboratory of Quantum Information of Chinese Academy of Sciences (CAS), University of Science and Technology of China, Hefei 230026, China
[4] CAS Center for Excellence in Quantum Information and Quantum Physics, University of Science and Technology of China, Hefei 230026, China

(Received 18 June 2020; revised manuscript received 16 August 2020; accepted manuscript online 28 September 2020)

We develop a new scheme of two-dimensional (2D) and three-dimensional (3D) atom localization via absorption and gain spectra of surface plasmon polaritons (SPPs) in a closed loop four-level atomic system. For the atom–field interaction, we construct a spatially dependent field by superimposing two (three) standing-wave fields (SWFs) in 2D (3D) atom localization, respectively. We achieve high-precision and high spatial resolution of an atom localization by appropriately adjusting the system parameters such as probe field detuning and phase shifts of the SWFs. The absorption and gain spectra are used to attain information about the position of an atom in SPPs. Our proposed scheme opens up a fascinating way to improve the atom localization that supplies some practical applications in a high-dimensional SPPs.

Keywords: atom localization, absorption and gain spectra, four-level atomic system

PACS: 42.50.Gy **DOI:** 10.1088/1674-1056/abbbeb

1. Introduction

The progress of quantum technologies plays a major role in the localization of moving atoms[1–3] through a standing-wave field (SWF) which is a wide area of research with applications in various fields, i.e., Bose–Einstein condensation,[4] laser cooling and neutral atom trapping,[5] atom lithography.[6] Multiple pioneering studies on atom localization have been proposed by laser manipulation, where the position of moving atom through an SWF can be determined by Ramsey interferometry,[7] performing a phase measurement on a probe field[8–10] and all other optical approaches.[11,12] Similarly, the atom localization has been introduced by using Autler–Townes microscopy technology,[13] spontaneous emission quenching,[14,15] and emission of photons by monitoring the amplitude and phase of the absorption spectra.[16,17]

In the current decade, the interest in high-dimensional (2D and 3D) atom localization has been increased due to its unique aspects and enormous applications. Ivanov and Rozhdestvensky[18] proposed a four-level tripod system and used the population of the excited states to determine the position of the 2D atom. They applied two orthogonal standing wave fields (OSWFs) to obtain a localized atom by adjusting the parametric conditions properly. Further, atom localization has been studied in the case of four- and five-level closed loops[19–21] and N-type[22] systems by monitoring the probe absorption and Raman gain process, respectively.

Furthermore, three mutually OSWFs have been used to achieve 3D atom localization in the M-type atomic system via calculating the EIT-based probe absorption.[23] In the four-level tripod-type system, the 3D atom localization has been investigated via excited-level population,[24] closed loop KR5 level system,[25] double two-level scheme,[26] and a closed loop four-level system.[27] On the basis of these findings, it is known that the spatial resolution of the atom location can be improved and that the maximum probability of finding an atom position could be achieved by considering a high dimensional scenario.

Recently, the surface plasmon polariton (SPP) absorption and dispersion spectra have been introduced in a one-dimensional atom localization.[28] SPPs possess a smaller wavelength than photons at the same frequency and have excellent nanoscale focusing light capabilities that leads to enhancing the localized field significantly.[29] Both theoretically and experimentally, the SPP dependent light has been used to manipulate elements such as planar metallic lenses, polarizers, and beam splitters.[30,31] Moreover, SPPs based optical circuits are promising as upcoming optical nanoscale circuits.[32–34] The SPPs including unidirectional SPP excitation and Airy SPP beam have important and interesting applications in improving the efficiency and lowering the cross-talk in plasmonic networks,[35] encoding the polarization information in SPPs, exhibiting the self-healing properties, which suggest the novel applications in plasmonic circuitry and surface optical manipulation.[36,37]

In this article, we consider a closed loop four-level atomic system for 2D and 3D atom localization in SPP. In addition,

*Project supported by CAS-TWAS Presidential fellowship and Chinese Scholarship Council (CSC) fellowship.
†Corresponding author. E-mail: amkhan@mail.ustc.edu.cn
‡Corresponding author. E-mail: mjansafi@mail.ustc.edu.cn
© 2020 Chinese Physical Society and IOP Publishing Ltd

we construct the spatially dependent SWFs in 2D and 3D for the atom–field interaction while measuring the absorption and gain spectra of SPP to localize the atom in high dimensions. Here, we choose the appropriate system parameters such as probe field detuning and phase shifts of the SWFs to achieve high-precision and high spatial resolution.

The outline of our article is as follows. In Section 2, we discuss the theoretical model and its solution for measuring the position-dependent absorption and gain spectra of SPP in a closed loop four-level atom. Detailed analysis and discussion of the absorption and gain spectra of SPP are presented in Section 3. Finally, in Section 4, we present our conclusions.

2. Model and theoretical approach

In this section, we describe our theoretical model which represents the dynamics of a closed loop four-level atomic system. The considered system consists of two lower states $|a\rangle$, $|b\rangle$ and two excited states $|c\rangle$, $|d\rangle$, as shown in Fig. 1 which displays the energy level diagram of the closed loop four-level atomic system. A probe field $E_{\rm p}$ having Rabi frequency $G_{\rm p}$ is applied between levels $|a\rangle \rightarrow |b\rangle$ with frequency ω_{ab}. A strong control traveling wave field $E_{\rm c}$ with Rabi frequency $G_{\rm c}$ is applied between transition $|b\rangle \rightarrow |c\rangle$ of frequency ω_{bc}. The position dependent standing wave field (SWF) $E_{\rm f}(r)$ with Rabi frequency $G_{\rm f}(r)$ and central frequency $\omega_{\rm f}$ is applied between transition $|c\rangle \rightarrow |d\rangle$ of frequency $\omega_{\rm cd}$. We use the generalized form of SWF $E_{\rm f}(r)$ obtained by superimposing two OSWFs (three OSWFs) in 2D (3D) as demonstrated by $E_{\rm f}(x,y)$ and $E_{\rm f}(x,y,z)$, respectively. Here, an additional signal weak field $E_{\rm s}$ with Rabi frequency $G_{\rm s}$ and central frequency $\omega_{\rm s}$ is applied between transition $|a\rangle \rightarrow |d\rangle$ to obtain a closed-loop configuration.

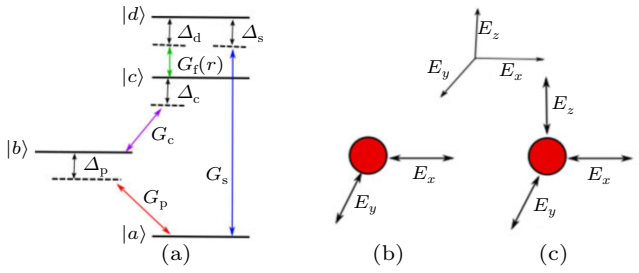


Fig. 1. (a) Schematic energy level diagram of a closed four-level atomic system. Here $G_{\rm p}$, $G_{\rm c}$, $G_{\rm f}(r)$, and $G_{\rm s}$ are the Rabi frequencies of probe field, control field, position-dependent OSWFs, and the weak signal field, respectively. Only one transition is controlled by each field. (b) Two OSWFs E_x and E_y orienting along the x-and y-directions form a 2D structure. (c) Three OSWFs E_x, E_y and E_z orienting along the x-, y-, and z-directions form a 3D structure.

Further, we assume that the center of mass position of the atom is constant along the direction of the standing waves due to the small kinetic energy of the atom as compared to the interaction energy of the applied field. We further note that our method is ideal for cold atoms because we do not consider atomic motion, and therefore there is no Doppler free broadening effect in our considered scheme. By using the Raman–Nath approximation,[38] we drop the kinetic energy term in the Hamiltonian. Hence, the interaction Hamiltonian of the system in rotating-wave and dipole approximations can be written as

$$H_{\rm int} = \Delta_{\rm p}|b\rangle\langle b| + (\Delta_{\rm p}+\Delta_{\rm c})|c\rangle\langle c| + (\Delta_{\rm p}+\Delta_{\rm c}+\Delta_{\rm f})|d\rangle\langle d| - (G_{\rm p}|b\rangle\langle a| + G_{\rm c}|c\rangle\langle b| + G_{\rm f}(r)|d\rangle\langle c| + G_{\rm s}|d\rangle\langle a| + {\rm h.c.}), \quad (1)$$

where $\Delta_{\rm p} = \omega_{ba} - \omega_{\rm p}$, $\Delta_{\rm c} = \omega_{cb} - \omega_{\rm c}$, $\Delta_{\rm f} = \omega_{dc} - \omega_{\rm f}$, and $\Delta_{\rm s} = \omega_{da} - \omega_{\rm s}$ denote the detuning of the applied fields for corresponding transitions, the respective Rabi frequencies ($G_{\rm p}$, $G_{\rm c}$, $G_{\rm f}(r)$, and $G_{\rm s}$) of the optical fields can be defined as $G_{\rm p} = \mu_{ba}E_{\rm p}/2\hbar$, $G_{\rm c} = \mu_{cb}E_{\rm c}/2\hbar$, $G_{\rm s} = \mu_{da}E_{\rm s}/2\hbar$, and $G_{\rm f}(r) = \mu_{dc}E_{\rm f}(r)/2\hbar$. Here, μ_{mn} represents the dipole matrix moment for the transition between $|m\rangle$ and $|n\rangle$. In this closed system case, the relationship $\omega_{\rm p} + \omega_{\rm c} + \omega_{\rm f} = \omega_{\rm s}$ is reduced to $\Delta_{\rm p} + \Delta_{\rm c} + \Delta_{\rm f} = \Delta_{\rm s}$.

The state vector of the system in our scenario can be defined as

$$|\psi(t)\rangle = C_1(t)|a\rangle + C_2(t)|b\rangle + C_3(t)|c\rangle + C_4(t)|d\rangle, \quad (2)$$

where C_i $(i = 1,2,3,4)$ represents the probability amplitudes. The rate equations of the corresponding probability amplitudes can be expressed by using Schrodinger equation as

$$\frac{\partial C_1}{\partial t} = {\rm i}G_{\rm p}C_2 + {\rm i}G_{\rm s}C_4, \quad (3a)$$

$$\frac{\partial C_2}{\partial t} = {\rm i}\left(-\Delta_{\rm p} + {\rm i}(\gamma_2 + \gamma_{\rm sp})\right)C_2 + {\rm i}G_{\rm p}C_1 + {\rm i}G_{\rm c}C_3, \quad (3b)$$

$$\frac{\partial C_3}{\partial t} = {\rm i}\left[-(\Delta_{\rm p}+\Delta_{\rm c}) + {\rm i}(\gamma_3 + \gamma_{\rm sp})\right]C_3 + {\rm i}G_{\rm c}C_2 + {\rm i}G_{\rm f}(r)C_4\,{\rm e}^{-{\rm i}\varphi}, \quad (3c)$$

$$\frac{\partial C_4}{\partial t} = {\rm i}\left[-(\Delta_{\rm p}+\Delta_{\rm c}+\Delta_{\rm f}) + {\rm i}(\gamma_4 + \gamma_{\rm sp})\right]C_4 + {\rm i}G_{\rm s}C_1, \quad (3d)$$

where γ_2, γ_3, and γ_4 are the atomic decay rates and $\gamma_{\rm sp}$ is the k-mode damping rate of SPP.

Further, we assume that both the signal and probe fields are very weak, so in this case, the atom's population is initially in level $|a\rangle$ (or $|C_1|^2 \cong 1$) and zero for the other levels. By using this assumption, we can derive the solution of Eq. (3) under the steady-state condition as

$$\rho_{ba} = C_2C_1^* = \frac{-G_{\rm c}G_{\rm s}G_{\rm f}(r) - \beta_2\beta_3G_{\rm p} + G_{\rm f}^2(r)G_{\rm p}}{\beta_1\beta_2\beta_3 - G_{\rm f}^2(r)\beta_1 - G_{\rm c}^2\beta_3}, \quad (4)$$

where $\beta_1 = -\Delta_{\rm p} + {\rm i}(\gamma_2 + \gamma_{\rm sp})$, $\beta_2 = -(\Delta_{\rm p}+\Delta_{\rm c}) + {\rm i}(\gamma_3 + \gamma_{\rm sp})$, and $\beta_3 = -(\Delta_{\rm p}+\Delta_{\rm c}+\Delta_{\rm f}) + {\rm i}(\gamma_4 + \gamma_{\rm sp})$.

The probe field is applied between levels $|b\rangle$ and $|a\rangle$ so that the optical susceptibility of the medium can be determined as

$$\chi_{\rm p} = K\frac{\rho_{ba}}{G_{\rm p}}, \quad (5)$$

where $K = N|D_{ba}|^2/2\hbar\varepsilon_0$. The probe susceptibility Eq. (5) has both a real and an imaginary part representing the effects of dispersion and absorption, respectively. In this article, we are only interested in the imaginary part of susceptibility that provides us the complete information about the absorption and gain spectra by applying the position dependent SWFs. The position-dependent normalized form of susceptibility is defined as

$$\chi' = \frac{\chi_p}{K}. \tag{6}$$

Furthermore, we use Maxwell's equations to derive the wave equations for a metallic conductor. The wave equations for the electric and magnetic fields with complex conductivity, permeability, and permittivity are defined in the metallic conductor as

$$\nabla^2 E_p = \mu\varepsilon\frac{\partial^2 E_p}{\partial t^2} + \mu\sigma\frac{\partial E_p}{\partial t}, \tag{7}$$

$$\nabla^2 B_p = \mu\varepsilon\frac{\partial^2 B_p}{\partial t^2} + \mu\sigma\frac{\partial B_p}{\partial t}, \tag{8}$$

where μ, ε, and σ are the permeability, permittivity, and conductivity of the metallic conductor, respectively. The conductivity relates the current density with the electric field. The above equations are solved in the form $E_p(r,t) = E_0 e^{ik_m r-(\omega_0+\Delta_p)t}$ and $B_p(r,t) = B_0 e^{ik_m r-(\omega_0+\Delta_p)t}$, where E_p represents the electric field having amplitude E_0 and B_p shows the magnetic field with amplitude B_0 of the metal. The k_m represents the complex wave vector of the electric and magnetic fields. The relationship of a complex wave vector is expressed as[39]

$$k_m^2 = \mu_0(\omega_0+\Delta_p)(g_1+ig_2), \tag{9}$$

with

$$g_1 = \varepsilon_0(\omega_0+\Delta_p)|\mu_m||\varepsilon_m|\cos(\theta_1+\theta_2) - |\mu_r||\sigma|\sin(\theta_2+\theta_3), \tag{10}$$

$$g_2 = \varepsilon_0(\omega_0+\Delta_p)|\mu_m||\varepsilon_m|\sin(\theta_1+\theta_2) + |\mu_m||\sigma|\cos(\theta_2+\theta_3), \tag{11}$$

where μ_0 and ε_0 are the permeability and permittivity of the free space and μ_m and ε_m are used for the metal. The expressions $\mu_m = \mu_0\mu_r$ and $\varepsilon_m = \varepsilon_0\varepsilon_r$ show the complex permeability and permittivity of the metal, whereas $\varepsilon_r = |\varepsilon_r|e^{i\theta_1}$, $\mu_r = |\mu_r|e^{i\theta_2}$, and $\sigma = |\sigma|e^{i\theta_3}$ represent the relative permittivity, permeability, and conductivity of the metal, respectively.

We define the SPP wave vector as $k_m = k_m^r + ik_m^i = k_0 n_r^m$, where $k_0 = \omega_p/c$ for $\omega_p = 2\pi c/\lambda$ represents the wave vector of the incident radiation and n_r^m is the refractive index of SPPs along the atomic metallic interface described by[28]

$$n_r^m = \pm\sqrt{\frac{\mu_0 c^2\left(g_1 \pm \sqrt{g_1^2+g_2^2}\right)}{2(\omega_0+\Delta_p)}} \pm i\sqrt{\frac{\mu_0 c^2\left(-g_1 \pm \sqrt{g_1^2+g_2^2}\right)}{2(\omega_0+\Delta_p)}}. \tag{12}$$

Using the above relationship of the refractive index, we obtain the expression for the SPP wave vector as

$$k_{sp} = k_0\sqrt{\frac{(n_r^m)^2(1+4\pi\chi')}{(n_r^m)^2+(1+4\pi\chi')}}, \tag{13}$$

where k_{sp} shows the complex wave vector of SPP related to the imaginary part of the susceptibility. Using this relation we investigate the atom localization at the interface of the metallic conductor and to atomic dielectric medium. The analytical relation of wave vector k_{sp} related to susceptibility Eq. (5) depends upon the control parameters, such as the intensities, phase shift, and the detuning of the applied fields. Therefore, we can obtain precise information about the atom's position by controlling these parameters.

3. Results and discussion

In this section, we describe our numerical results of the position dependent probe absorption and gain spectra of SPP. We briefly discuss the importance of controlling parameters of the applied fields for the 2D and 3D atom localization.

In this closed loop configuration $|a\rangle \to |b\rangle \to |c\rangle \to |d\rangle \to |a\rangle$, the spatially dependent SPP probe absorption and gain spectra are used to obtain the atom localization by applying the appropriate field parameters. Further, we assume that the collective phase of the applied fields is $\phi = 0$, because it provides significantly high absorption and gain spectra.[20] In atomic units, we use the following parameters: $\hbar = 1$, $\varepsilon_r = \mu_r = 1$, $\lambda = 1$ Å, and $c = 137$. In our scheme, we choose distinct values of probe field detuning and the phase shifts of the SWFs in order to attain 2D and 3D atom localization in the SSP.

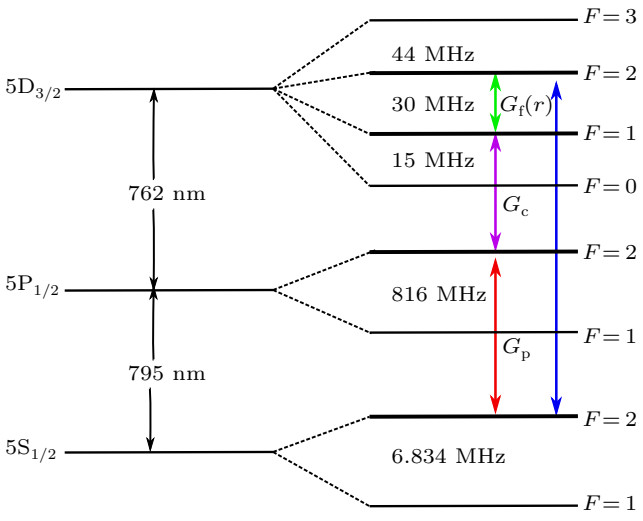


Fig. 2. Possible experimental scheme for a closed loop four-level ^{87}Rb atomic system.

3.1. Possible experimental realization

The proposed four-level atom-field system for 2D (3D) atom localization is a simple scheme that can be realized experimentally. In this subsection, we briefly discuss the possible experimental realization of our proposed scheme. We consider ^{87}Rb cold atom as a suitable choice with the allowed transitions $5S_{1/2}$–$5P_{1/2}$–$5D_{3/2}$,[40] which are assigned as follows: $|a\rangle = |5S_{1/2}, F = 2\rangle$, $|b\rangle = |5P_{1/2}, F = 2\rangle$, $|c\rangle = |5D_{3/2}, F = 1\rangle$, and $|d\rangle = |5D_{3/2}, F = 2\rangle$. Figure 2 shows the experimental realization of our proposed scheme, where γ_2, γ_3, and γ_4 are the atomic decay rates whose values are scaled in units of $\gamma = 2\pi \times 6.07$ MHz.[41] Further, to eliminate the Doppler broadening effect, the atoms should be trapped and cooled by utilizing magneto-optical trap technology.[42] The probe and control fields can be obtained from external cavity diode lasers.

For this experimental scheme, the cold ^{87}Rb atom, moving along the z axis, passes through the intersection region of two (three) OSWFs oriented effectively along the x and y axes (x, y, and z axes). The composition of the two (three) OSWFs can be obtained by combining four (six) identical fields along x- and y-directions in 2D and x-, y-, and z-directions in 3D case. Each SWF is a superposition of two more SWFs in each direction. The probe absorption and gain observed at appropriate frequencies are position dependent. Such position-dependent probe absorption and gain can be reflected by a standard spectroscopic method, which may be realized via the experiment proposed by Proite *et al.*[43]

3.2. The 2D atom localization

In this subsection, we present our results of absorption and gain spectra of SPP in two-dimensional plane. In this case, the SWFs are the resultant superposition field of two OSWFs $E_f(x)$ and $E_f(y)$, and their corresponding Rabi frequencies are defined by[44]

$$G_f(x,y) = G_f(x) + G_f(y), \tag{14}$$

with

$$G_f(x) = G_1 \left[\sin(k_1 x + \eta) + \sin(k_2 x)\right], \tag{15}$$

$$G_f(y) = G_2 \left[\sin(k_3 y + \zeta) + \sin(k_4 y)\right], \tag{16}$$

where k_i ($i = 1,2,3,4$) is the wave vector related with wavelength λ_i as $k_i = 2\pi/\lambda_i$. The phase shifts parameters η and ζ are related with SWFs wave vectors k_1 and k_3, respectively.

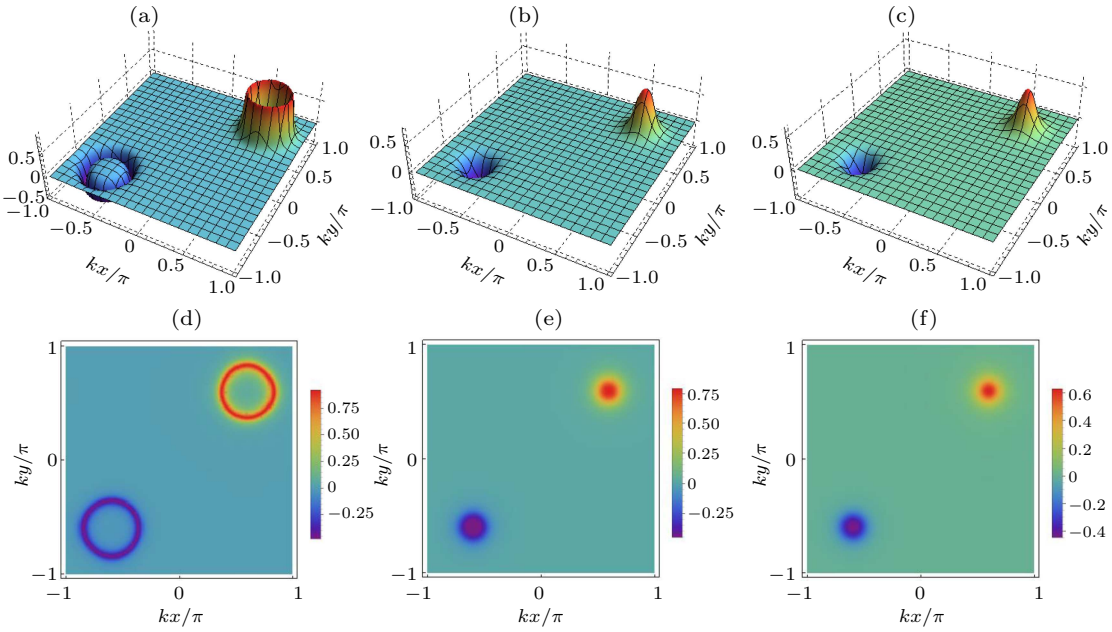


Fig. 3. The normalized probe absorption and gain spectra of SPP Im[k_{sp}] as a function of (kx, ky) for different values of probe field detuning: (a) $\Delta_p = 60\gamma$, (b) $\Delta_p = 66\gamma$, and (c) $\Delta_p = 72\gamma$. All other parameters are selected as $\Delta_c = 20\gamma$, $\Delta_f = -5\gamma$, $\sigma = 10$ M·S/m, $\theta_1 = \theta_2 = \theta_3 = 0$, $\gamma_2 = 0.003\gamma$, $\gamma_3 = 0.75\gamma$, $\gamma_4 = 0.8\gamma$, $\gamma_{sp} = 0.8\gamma$, $G_p = 0.1\gamma$, $G_c = 20\gamma$, $G_1 = G_2 = 20\gamma$, $G_s = 0.1\gamma$, $\eta = 0$, $\zeta = 0$, and $k_1 = k_3 = 0.5k$. (d)–(f) The corresponding density plots in the xy-plane.

Firstly, we examine the probe field detuning effect to study the absorption and gain spectra of SPP. Figures 3(a)–3(c) show the absorption and gain spectra of SPP versus the normalized position (kx, ky) for various values of probe field detuning (Δ_p) while keeping other parameters fixed. For the value of $\Delta_p = 60\gamma$, we see the crater-like structure in the first quadrant which shows the absorption whereas an inverted crater-like structure is obtained in the third quadrant which represents the gain as shown in Fig. 3(a). Further, by increasing the probe field detuning to $\Delta_p = 66\gamma$, we observe a spike-like structure as depicted in Fig. 3(b) that shows the absorption spectrum in the first quadrant whereas the gain peak is

viewed in the third quadrant as an inverted spike-like structure. Furthermore, if we increase the probe field detuning to $\Delta_p = 72\gamma$, in the first quadrant we obtain the spike-like structure that shows the absorption spectrum and inverted spike-like structure that represents the gain spectrum in the third quadrant as shown in Fig. 3(c). The density plots in Figs. 3(d)–3(f) provide a clear view of absorption and gain spectra of SPP in xy-plane for the different values of the probe field detuning.

Moreover, we examine the relative phase effect of SWFs on the probe absorption and gain spectra of SPP. Figures 4(a)–4(c) show the probe absorption and gain spectra of SPP versus normalized position (kx, ky) for different SWFs phase shifts values. For the phase shifts values $\eta = \zeta = 0$, we obtain a spike-like structure in the first quadrant which shows the absorption spectrum whereas the inverted spike-like structure in the third quadrant represents the gain spectrum, as shown in Fig. 4(a) which is similar to the results depicted in Fig. 3(c). If we change the phase shifts values to $\eta = \zeta = \pi/4$, then, in this case, we only get the absorption spectrum in the first quadrant, which is a crater-like structure as shown in Fig. 4(b). In this scenario, we only get the absorption spectrum having very poor resolution. Now to attain a high-precision and high-resolution absorption spectrum, we change the phase shift values as $\eta = \zeta = \pi/2$. In this case, only the absorption peak in the first quadrant is shown by a spike-like structure having a high-precision and high spatial resolution, as depicted in Fig. 4(c). Figures 4(d)–4(f) show the corresponding density plots of the absorption and gain spectra of SPP in the xy-plane for the different phase shifts values of SWFs.

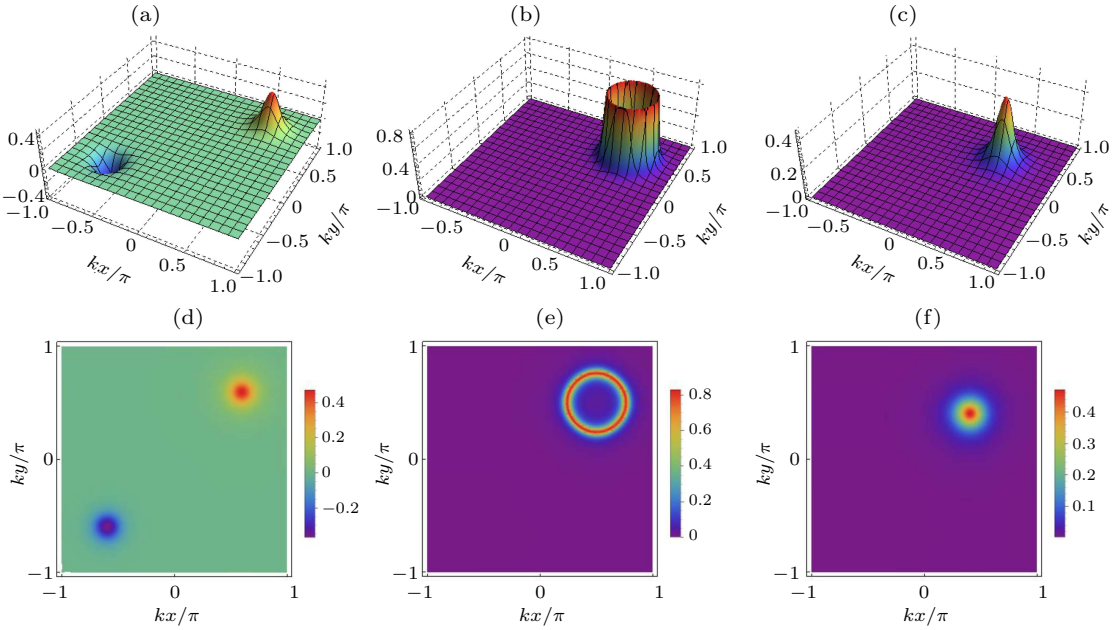


Fig. 4. The normalized probe absorption and gain spectra of SPP Im[k_{sp}] as a function of (kx,ky) for different values of phase shifts: (a) $\eta = \zeta = 0$, (b) $\eta = \zeta = \pi/4$, and (c) $\eta = \zeta = \pi/2$, $\Delta_p = 70\gamma$. Other parameters are the same as those in Fig. 3. (d)–(f) The corresponding density plots in the xy-plane.

In this subsection, we investigate the effect of probe field detuning and phase shifts values in calculating the absorption and gain spectra of SPP in the xy-plane. In both cases, we find that the absorption and gain spectra are highly dependent on the probe field detuning and the phase shifts. In the probe field detuning case, we have analyzed that the field is absorbed in the first quadrant ($kx, ky = \pi/2, \pi/2$) which is amplified in the third quadrant ($kx, ky = -\pi/2, -\pi/2$). Moreover, for the phase shifts values $\eta = \zeta = \pi/4$ and $\eta = \zeta = \pi/2$, we only get the absorption peak in the first quadrant which provides a high probability of an atom in the xy-plane.

3.3. The 3D atom localization

In this subsection, we present our results of absorption and gain spectra of SPP in three-dimensional space. In this case, the SWFs are the resultant superposition field of three sub-fields $E_f(x)$ and $E_f(y)$, and their corresponding Rabi frequencies are described as

$$G_f(x,y,z) = G_f(x) + G_f(y) + G_f(z), \tag{17}$$

where $G_f(x)$ and $G_f(y)$ are the Rabi frequencies defined in Eqs. (15) and (16), and $G_f(z)$ is given by

$$G_f(z) = G_2\left[\sin(k_5 z + \xi) + \sin(k_6 z)\right], \tag{18}$$

where ξ is the phase shift parametersrelated with SWFs wave vector k_5.

We analyze the probe field detuning effect to examine the absorption and gain spectra of the SPP in 3D space. In order to calculate the precise position and high resolution absorption and gain spectra of SPP, we choose the appropriate values for the probe field detuning while the other parameters remain

fixed. In this 3D case, we apply the same values of probe field detuning as we have already discussed in Subsection 3.2.Figure 5(a) shows the result for the probe field detuning $\Delta_p = 60\gamma$. In this case, we obtain two spherical bodies which represent the absorption spectrum in the first quadrant and gain spectrum in the third quadrant, respectively. Now increasing the probe field detuning to $\Delta_p = 66\gamma$ (Fig. 5(b)) and $\Delta_p = 72\gamma$ (Fig. 5(c)), we observe two spherical bodies showing absorption and gain spectra in the first and third quadrants, respectively. In this case, we find that by increasing the probe field detuning we obtain high-precision and high-resolution absorption and gain spectra of SPP which provide a high probability of atom localization.

Furthermore, we discuss the effect of the relative phase shifts of SWFs. The results of absorption and gain spectra of SPP in 3D for different phase shifts values (η, ζ, ξ) of SWFs, with other parameters fixed are shown in Figs. 6(a)–6(c). For the phase shift values $(\eta = 0, \zeta = 0, \xi = 0)$ we obtain two spherical bodies which show high-precision absorption and gain spectra of SPP, the same as those shown in Fig. 5(c). If we change the phase shifts of SWFs to $(\eta = \pi/4, \zeta = \pi/4, \xi = \pi/4)$, we only get one spherical body which represents the absorption spectrum of SPP in the first quadrant as shown in Fig. 6(b). In this case, the absorption spectrum observed in the first quadrant has poor resolution. High-precision and high resolution of the atom position can be achieved for the SWFs phase shifts $(\eta = \pi/2, \zeta = \pi/2, \xi = \pi/2)$. In this case, the spherical body in the first quadrant shows the absorption spectrum of SPP, which provides the high probability of atom localization in the first quadrant.

In this subsection, we introduce the effect of probe field detuning and phase shifts of SWFs to study the absorption and gain spectra of SPP in 3D. We have observed that by increasing the probe field detuning, one can achieve high-precision and high resolution of the atom location in 3D space. The probe field absorption in the first quadrant shows the atom localization in the region $(kx, ky, kz = \pi/2, \pi/2, \pi/2)$, whereas the probe field amplification in the third quadrant shows the atom localization in the region $(kx, ky, kz = -\pi/2, -\pi/2, -\pi/2)$. By applying the suitable phase shifts of SWFs, we obtain only the absorption of the probe field in the first quadrant with high probability of an atom localization in the region $(kx, ky, kz = \pi/2, \pi/2, \pi/2)$.

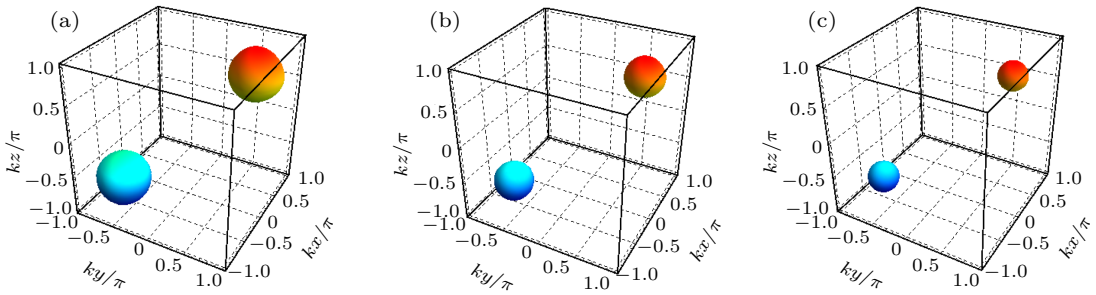


Fig. 5. The normalized probe absorption and gain spectra of SPP Im$[k_{sp}]$ as a function of (kx, ky, ky) for different values of probe field detuning: (a) $\Delta_p = 60\gamma$, (b) $\Delta_p = 66\gamma$, and (c) $\Delta_p = 72\gamma$, $G_1 = G_2 = G_3 = 15\gamma$, $\eta = 0$, $\zeta = 0$, $\xi = 0$, and $k_1 = k_3 = k_5 = 0.5k$. Other parameters are the same as those in Fig. 3.

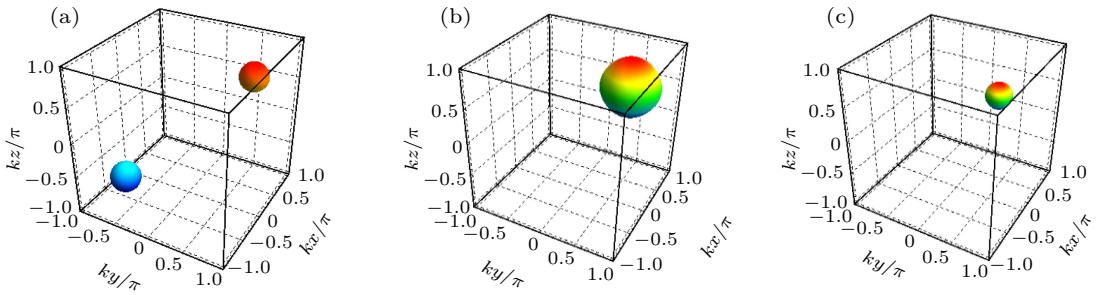


Fig. 6. The normalized probe absorption and gain spectra of SPP Im$[k_{sp}]$ as a function of (kx, ky, kz) for different values of phase shifts: (a) $\eta = \zeta = \xi = 0$, (b) $\eta = \zeta = \xi = \pi/4$, and (c) $\eta = \zeta = \xi = \pi/2$, $\Delta_p = 70\gamma$, $k_1 = k_3 = k_5 = 0.5k$. Other parameters are the same as those in Fig. 3.

4. Conclusion

We have studied 2D and 3D atom localization in a closed loop four-level atomic system by analyzing the absorption and gain spectra of SPP. By choosing the appropriate values of the probe field detuning, we have achieved high-precision and high spatial resolution of atom localization by quantifying the normalized absorption and gain spectra. The observed two peaks show the absorption and gain spectra in the first and third quadrants, respectively. Further, for the zero phase shifts of SWFs, both absorption and gain spectra are shown, whereas the gain spectrum disappears for non-zero phase shifts of SWFs. In this scenario, a single peak of absorption spectrum

gives the maximum probability of an atom localization. Moreover, 3D atom localization shows the same behavior like 2D one while controlling both the probe field detuning and phase shifts of SWFs.

References

[1] Kapale K T, Qamar S and Zubairy M S 2003 *Phys. Rev. A* **67** 023805
[2] Mompart J, Ahufinger V and Birkl G 2009 *Phys. Rev. A* **79** 053638
[3] Evers J, Qamar S and Zubairy M S 2007 *Phys. Rev. A* **75** 053809
[4] Anderson M H, Ensher J R, Matthews M R, Wieman C E and Cornell E A 1995 *Science* **269** 198
[5] Phillips W D 1998 *Rev. Mod. Phys.* **70** 721
[6] Johnson K S, Thywissen J H, Dekker N H, Berggren K K, Chu A P, Younkin R and Prentiss M 1998 *Science* **280** 1583
[7] Le Kien F, Rempe G, Schleich W P and Zubairy M S 1997 *Phys. Rev. A* **56** 2972
[8] Storey P, Collett M and Walls D 1992 *Phys. Rev. Lett.* **68** 472
[9] Kunze S, Dieckmann K and Rempe G 1997 *Phys. Rev. Lett.* **78** 2038
[10] Quadt R, Collett M and Walls D F 1995 *Phys. Rev. Lett.* **74** 351
[11] Thomas J E 1989 *Opt. Lett.* **14** 1186
[12] Stokes K D, Schnurr C, Gardner J R, Marable M, Welch G R and Thomas J E 1991 *Phys. Rev. Lett.* **67** 1997
[13] Qamar S, Zhu S Y and Zubairy M 2000 *Opt. Commun.* **176** 409
[14] Wan R G, Zhang T Y and Kou J 2013 *Phys. Rev. A* **87** 043816
[15] Wan R G and Zhang T Y 2011 *Opt. Express* **19** 25823
[16] Qamar S, Zhu S Y and Zubairy M S 2000 *Phys. Rev. A* **61** 063806
[17] Sahrai M, Tajalli H, Kapale K T and Zubairy M S 2005 *Phys. Rev. A* **72** 013820
[18] Ivanov V and Rozhdestvensky Y 2010 *Phys. Rev. A* **81** 033809
[19] Ding C, Li J, Yang X, Zhang D and Xiong H 2011 *Phys. Rev. A* **84** 043840
[20] Shui T, Wang Z and Yu B 2014 *Phys. Lett. A* **378** 235
[21] Singh N and Wasan A 2018 *J. Opt. Soc. Am. B: Opt. Phys.* **35** 1318
[22] Rahmatullah, Wahab A and Qamar S 2014 *Laser Phys. Lett.* **11** 045202
[23] Qi Y, Zhou F, Huang T, Niu Y and Gong S 2012 *J. Mod. Opt.* **59** 1092
[24] Ivanov V S, Rozhdestvensky Y V and Suominen K A 2014 *Phys. Rev. A* **90** 063802
[25] Hamedi H R and Juzeliūnas G 2016 *Phys. Rev. A* **94** 013842
[26] Zhu Z, Yang W X, Xie X T, Liu S, Liu S and Lee R K 2016 *Phys. Rev. A* **94** 013826
[27] Mao Y and Wu J 2017 *J. Opt. Soc. Am. B* **34** 1070
[28] Shah S A, Ullah S, Idrees M, Bacha B A, Ali A and Ullah A 2019 *Phys. Scr.* **94** 035401
[29] Qamar S, Mehmood A and Qamar S 2009 *Phys. Rev. A* **79** 033848
[30] Raether H 1988 *Surface Plasmons on Smooth and Rough Surfaces and on Gratings* Vol. 111, 1st Ed. (Heidelberg: Springer) p. X, 136
[31] Gramotnev D K and Bozhevolnyi S I 2010 *Nat. Photon.* **4** 83
[32] Maier S A, Brongersma M L, Kik P G, Meltzer S, Requicha A A G and Atwater H A 2001 *Adv. Mater.* **13** 1501
[33] Xu T, Du C, Wang C and Luo X 2007 *Appl. Phys. Lett.* **91** 201501
[34] Verslegers L, Catrysse P B, Yu Z and Fan S 2009 *Appl. Phys. Lett.* **95** 071112
[35] Lin J, Mueller J P, Wang Q, Yuan G, Antoniou N, Yuan X C and Capasso F 2013 *Science* **340** 331
[36] Minovich, Alexander and Klein, Angela E. and Janunts, Norik and Pertsch, Thomas and Neshev, Dragomir N. and Kivshar, Yuri S. 2011 *Phys. Rev. Lett.* **107** 116802
[37] Yin X, Chen L and Li X 2018 *Opt. Express* **26** 23251
[38] Meystre P and Sargent M 2007 *Elements of Quantum Optics* (Berlin: Springer)
[39] Khan N, Amin Bacha B, Iqbal A, Ur Rahman A and Afaq A 2017 *Phys. Rev. A* **96** 013848
[40] Steck D A 2016 http://steck.us/alkalidata
[41] Zhang D, Yu R, Sun Z, Ding C and Zubairy M S 2017 *J. Phys. B: At. Mol. Opt. Phys.* **51** 025501
[42] Uhlenberg G and Dirscherl J and Walther H 2000 *Phys. Rev. A* **62** 063404
[43] Proite N A, Simmons Z J and Yavuz D D 2011 *Phys. Rev. A* **83** 041803
[44] Wahab A, Rahmatullah and Qamar S 2016 *J. Mod. Opt.* **63** 1059